Design and Implementation of the Control System for a Hybrid Excitation Synchronous Machine

Guo Xinjun[*], Huang Mingming, Huang Quanzhen, Liu Yuping and Lina

School of Electrical Information Engineering, Henan Institute of Engineering, Zhengzhou, 451191, China

Abstract: This paper proposed a novel kind of hybrid excitation synchronous machine (HESM) driving system, which possesses the properties of low speed high torque and has wide speed range. Firstly, the construction, the basic working principle and the concept of design were overviewed. Following this , the principle of two-speed-region control algorithm was presented based on the space voltage vector control. The proposed control algorithm includes two aspects. 1) In the low speed region, the current control strategy was adopted with or without excitation current for adjusting speed according to the load of HESM. 2) In the high speed region, the current control strategy adopts a combination strategy of holding q-axis components of Back-EMF unchanged and the copper loss minimization algorithm. The proposed methods were verified by the contrastive simulations and the experimental results through different current control methods.

Keywords: Flux weakening control, hybrid excitation synchronous machine, vector control, wide speed range.

1. INTRODUCTION

Hybrid excitation synchronous machine (HESM) is a wide speed range machine consistings of the permanent magnet synchronous motor (PMSM). Its inner side contains two magnetic potential sources: permanent magnet and excitation windings. The permanent magnet in the motor generates a main air gap magnetic flux and excitation winding generates an auxiliary air gap magnetic flux. Because of excitation windings, it can increase or reduce the air-gap magnetic field by changing the size and direction of the current, which make the motor have the characteristics of a low speed high torque and a wide speed operation range. Therefore , its application is very extensive and valuable in industrial and agricultural production, and is particularly suitable for machines which need high speed operation capability, like the electric vehicles, machine tools, servo systems, and so on [1-3].

Because of structural and performance similarities in HESM and PMSM, and updated control technology and products of PMSM, the HESM can fully reference the basic principles and control methods of the PMSM [4-7]. But, the HESM generates an additional controllable excitation current to adjust the air gap magnetic field of the motor, therefore a reasonable allocation of the excitation current and the armature currents must be considered to achieve optimal control of efficiency, static and dynamic characteristics. HESM's basic control principle is to make the motor acquire operation capabilities of a higher starting torque and low speed high torque by increasing air gas magnetic field intensity (Combination of excitation current and the d-axis

current for flux enhancement) or by using non-excitation method for adjusting speed under the rated speed. After the motor speed exceeds the flux weakening base speed (typically rated speed), its back-EMF approaches to the DC bus voltage and if the speed needs to be further improved the flux weakening control method is adopted. Currently, the research papers on HESM control system mainly include the following. A hybrid excitation brushless DC motor fuzzy control scheme was presented by academician Qingquan Chen, used to regulate the armature current and excitation current by using the fuzzy controller [8]. A common coordinate system based dynamic vector control model was proposed by Japanese scholars Shinji Shinnaka [9], and a copper loss minimization vector control method based on id=0 was proposed for the non-salient pole HESM [10]. A HESM control method was simplified by Qianfan Zhang after which, the quantity and direction of coil's current are controlled by the stator winding current and the back EMF which are the same phase of square wave [11]. In the paper [12], professor Deng proposed a novel maximum torque/copper loss control method. A relatively simple method for partitioning control strategy and its implementation was presented by Dr. Yang Chengfeng, and the no excitation current control mode was also compared [13]. All of the above documents did not consider the role of d-axis current for regulated speed, therefore, it is very difficult to obtain adequate the motor efficiency and speed range.

In order to obtain the desired properties of low speed high toque and wide speed range operation, this paper proposed a novel control strategy based on two-speed region control, with or without excitation current for regulating speed in the low speed region, and adopted flux weakening control based on copper loss minimization method in the high speed region. Designing the flux weakening control

*Address correspondence to this author at the No. 1 Xianghe Road, Longhu Town, Xinzheng City, Zhenzhou City, China, Postcard: 451191; Tel: 13526587276; E-mail: hngcxy_hmm@163.com
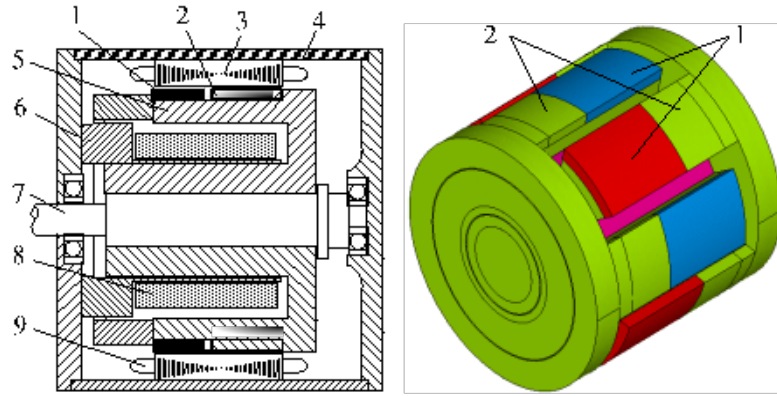
(a) The structure of HESM　　　　　(b) The rotor

1. permanent magnet; 2. the iron pole; 3. the iron core of stator; 4. the outer covering; 5. the claw pole; 6. the cover; 7. the axis; 8.the exciting winding; 9. the armature winding.

Fig. (1). The model of HESM.

algorithm in high speed region is an important feature of the HESM control system. According to the flux weakening operating characteristics of HESM in the high speed region and based on vector control of two current allocation algorithms, the combination of the excitation current and the d-axis current for air-gas magnetic flux regulation, and the excitation current for air-gas magnetic flux regulation, were proposed. Comparing the above two algorithms with no flux weakening control method in the simulation, the results show that the suggested methods, based on copper loss minimization, combined the d-axis currents and excitation currents for flux weakening control, had much higher speed range than another two methods. Finally, the experiment proved the effectiveness of the proposed control methods.

2. THE FRAMEWORK AND MATHEMATIC MODEL OF HESM

The motor of the proposed HESM drive system is a claw-pole asymmetric interlaced HESM, which is shown in Fig. (**1**). The motor has dual stator structure and outer stator is similar to the general PMSM stator. Three-phase armature windings are installed inside and a chute structure is used to reduce cogging torque. Inner stator is consists of a coil with iron core, namely excitation coil, which is fixed to the end cap of the motor. The rotor has a claw-pole shape. The magnetically conductive irons (namely iron core pole) and the permanent magnets (*i.e.*, permanent magnet pole) are placed on the adjacent claw-pole staggered. (AUTHOR: Should this word "staggered" be removed?) In the inner surface of HESM, magnetic flux generated by permanent magnet pole is almost unchanged during motor operation. Except for some of the magnetic flux leakage. The magnetic flux flows in the path as follows:

permanent magnet N-pole → air gap → stator teeth → stator iron core → stator teeth →air gap → adjacent permanent magnet S-pole → S-pole claw pole → magnet yoke disc of claw pole → rotor magnet yoke → additional air gap in rotor → inner stator core → claw pole yoke ring → N-pole claw pole → permanent magnet N-pole.

The magnetic flux generated by each current component flows with least reluctance, and their magnetic flux path is almost same with the permanent magnet. However, their difference is mainly due to the fact that the most magnetic flux generated by the currents is bypassed through the high magnetic conductivity material (iron core) paralleled with permanent magnet., thus it does not pass the permanent magnet and will not cause permanent damage to permanent magnets. Due to the low reluctance of the whole magnetic circuit , a good magnetic-flux-adjusting effect is obtained by regulating excitation current and the *d*-axis current.

In summary, the paths of magnetic flux generated by the permanent magnet, the excitation current and the *d*-axis current are substantially identical. Therefore, the air-gas magnetic field of HESM can be approximated linear superimposed, and can also be adjusted effectively by changing the size and direction of excitation current and the d-axis current.

To simplify the analysis, the effects of the armature voltage, harmonic component, temperature change, iron loss, stray loss, and magnetic saturation were ignored when mathematic model and driver system model were built according to the above illustrated HESM structure. Several basic equations of mathematic model of HESM can be obtained as follows:

Circuit equation:

$$
\begin{bmatrix} u_d \\ u_q \\ u_f \end{bmatrix} = \begin{bmatrix} R_s + sL_d & -\omega_e L_q & sM_{sf} \\ \omega_e L_d & R_s + sL_q & \omega_e M_{sf} \\ sM_{sf} & 0 & R_f + sL_f \end{bmatrix} \begin{bmatrix} i_d \\ i_q \\ i_f \end{bmatrix}
$$
$$
+ \begin{bmatrix} 0 \\ \omega_e \psi_{pm} \\ 0 \end{bmatrix} \tag{1}
$$

Flux linkage equation:

$$
\begin{bmatrix} \psi_d \\ \psi_q \end{bmatrix} = \begin{bmatrix} L_d & 0 & M_{sf} \\ 0 & L_q & 0 \end{bmatrix} \begin{bmatrix} i_d \\ i_q \\ i_f \end{bmatrix} + \begin{bmatrix} \psi_{pm} \\ 0 \end{bmatrix} \tag{2}
$$

Torque equation:

$$
\begin{aligned}
T_e &= \frac{3}{2} p(i_q \psi_d - i_d \psi_q) \\
&= \frac{3}{2} p i_q [\psi_{pm} + i_d(L_d - L_q) + M_{sf} i_f]
\end{aligned} \tag{3}
$$

In the formula (1) - (3), the symbol meanings are as following:

u_d-- d-axis voltage component,

u_q-- q-axis voltage component,

i_d-- d-axis current component,

i_q-- q-axis current component,

ψ_d-- d-axis flux linkage,

ψ_q-- q-axis flux linkage,

ψ_{pm}-- The flux linkage generated by permanent magnet ,

u_f-- excitation voltage,

i_f-- excitation current,

R_s -- armature resistance,

R_f-- excitation winding resistance,

L_d-- d-axis inductance,

L_q-- q-axis inductance,

M_{sf}-- mutual inductance between armature windings and excitation windings,

ω_e -- electrical angular velocity,

p -- number of pole pairs of the motor,

T_e-- electromagnetic torque.

3. THE PRINCIPLE OF TWO-SPEED-REGION CONTROL

According to the HESM's speed operation range, the proposed control strategy divides the whole speed range into two regions. Region I ($n_r \le n_b$, n_r is the rotor speed, n_b is the base speed) is the low speed region, uses the method that adopts current with or without excitation for adjusting speed and   region II($n_r > n_b$) is the high speed region, adopting flux weakening control by excitation current and d-axial current for adjusting speed based on copper loss minimization.

3.1. The Control Algorithms in the Low Speed Region

When the HESM's speed is less than or equal to the base speed, it adopts current with or without excitation, for adjusting speed according to its load torque. In order to simplify

the control algorithms, and to improve the reliability of HESM's operation, a vector control algorithm based on i_d=0 was adopted due to the inductor values L_d, L_q, and M_{sf} changed with the currents i_d, i_q, and $i_{f,}$. The torque equation can be obtained as:

$$
T_{eref} = \frac{3}{2} p[\psi_{pm} + M_{sf} i_{fref}] i_{qref} \tag{4}
$$

Where, T_{eref} is the reference value of electromagnetic torque, i_{qref} is the reference value of q-axis current component, i_{fref} is the reference value of excitation current. When T_{eref} is less than or equal to the base value

$$
T_N = \frac{3}{2} p\psi_{pm} I_{qN} \tag{5}
$$

Where, I_{qN} is the base value of q-axis current. In this condition, no excitation current is needed for speed regulation, only the current i_{qref} is required to be adjusted according to the value of T_{eref} changed during HESM's operation, that is

$$
i_{qref} = \frac{2T_{eref}}{3p\psi_{pm}} \tag{6}
$$

Such, when T_{eref} is larger, and

$$
T_{eref} > \frac{3}{2} p\psi_{pm} I_{qN} \tag{7}
$$

After this, i_{qref} is adjusted to maintain stable operation of HESM which will lead to motor overheat. By adopting flux strengthening control, let $i_{qref}=I_{qN}$, and T_{eref} can be obtained by

$$
T_{eref} = \frac{3}{2} p\psi_{pm} I_{qN} + \frac{3}{2} pM_{sf} i_{fref} I_{qN} \tag{8}
$$

then

$$
i_{fref} = \frac{2T_{eref} - 3p\psi_{pm} I_{qN}}{3pM_{sf} I_{qN}} \tag{9}
$$

In summary, when $T_{eref} \le T_N$, the reference currents can be obtained as:

$$
\begin{cases} i_{fref} = 0 \\ i_{dref} = 0 \\ i_{qref} = \frac{2T_{eref}}{3p\psi_{pm}} \end{cases} \tag{10}
$$

when $T_{eref} > T_N$, and the reference currents are

$$
\begin{cases} i_{fref} = \frac{2T_{eref} - 3p\psi_{pm} I_{qN}}{3pM_{sf} I_{qN}} \\ i_{dref} = 0 \\ i_{qref} = I_{qN} \end{cases} \tag{11}
$$

3.2. Flux Weakening Control Algorithms For HESM

The motor enters into the high-speed operation mode when the HESM's speed n_r exceeds the base speed n_b, and the back-EMF approaches to the DC-bus voltage (U_{dc}). To further elevate the speed, flux weakening methods must be used. The regulation of the armature current and excitation current is restricted to the voltage limit ring, which is similar to PMSM flux weakening control method in terms of constant power region. When the operation is stable, the voltage vector magnitudes have to meet the following condition:

$$u_s^2 = u_d^2 + u_q^2 \leq U_{lim}^2 \tag{12}$$

Where, U_{lim} is the voltage vector limit whose value depends on U_{dc} of the drive circuit. In the formula (12), u_s depends on u_q, while u_q is determined by E_q (q-axis component of the back EMF). According to the above analysis, a flux weakening control method based on maintaining the back EMF invariable is presented, *i.e.*

$$E_q = E_{base} \tag{13}$$

Where, E_{base} is the corresponding back-EMF in the no-load condition when n_r reaches n_b.

$$E_{base} = p n_{Bdec} \psi_{pm} \pi / 30 \tag{14}$$

The expression of E_q is the following as

$$E_q = \frac{p\pi n_r}{30} (\psi_{pm} + i_d L_d + i_f M_{sf}) \tag{15}$$

Where, it is known that n_r is the linear relationship with E_q when $i_d = i_f = 0$. Therefore, when using conventional vector control, the maximum speed n_{max} in no-load and no-excitation current are also in a linear relationship with U_{dc} Where, n_b is restricted by n_{max}, while n_{max} can be obtained by experiments with $i_d=i_f=0$ vector control in the no-load. Following this, the relationships of n_b, n_{max} and U_{dc} can be expressed using the following formula

$$\begin{cases} n_{max} = k_v U_{dc} + N_0 \\ n_b = k_b n_{max} \end{cases} \tag{16}$$

Where, for the experimental prototype, the maximum speed to voltage ratio coefficient takes $k_v = 5.69$, offset value $N_0 = -13$. To ensure the utilization rate of DC bus voltage and the motor efficiency in flux weakening operating state, the flux weakening base speed coefficient k_b is set a range of 0.7~0.9, where, $k_b = 0.75$. Therefore, when the DC bus voltage value IS $U_{dc} = 300V$, then $n_b = 1270rpm$.

Therefore, in order to maintain the back EMF with a higher value and unchanged in-flux weakening running states, and to combine equation (13~16), it is assumed that:

$$\begin{cases} i_d = i_{dref} \\ i_f = i_{fref} \end{cases} \tag{17}$$

Where, i_{dref}, and i_{fref} are the reference values of d-axis currents and excitation currents, respectively. Thus, it can be obtained

$$(L_d i_{dref} + M_{sf} i_{fref}) = \frac{\psi_{pm}(n_b - n_r)}{n_r} \tag{18}$$

The copper loss equation in high speed regions can be obtained by using copper loss minimization principle to carry out flux weakening control

$$P_{cu\text{-}ref} = \frac{3}{2} i_{dref}^2 R_s + i_{fref}^2 R_f \tag{19}$$

Where, in order to simplify the computation, the value of i_{qref} is directly determined by the reference electromagnetic torque T_{eref} given as output by speed controller. Therefore, it does not include the copper loss produced by q-axis component current i_{qref} in the formula (19), and

$$i_{qref} = k_i T_{eref} \tag{20}$$

Where, k_i is the q-axis current to torque ratio coefficient. Combining equation (18) and (19), the Lagrange multiplier was adopted to determine the reference current values based on copper loss minimization control method.

$$L(i_{dref}, i_{fref}, \lambda) = P_{cu\_ref} + \lambda[(L_d i_{dref} + M_{sf} i_{fref}) - \frac{\psi_{pm}(n_b - n_r)}{n_r}] \tag{21}$$

To solve partial derivatives of i_{dref}, i_{fref} and λ for equation (21), respectively:

$$\begin{cases} \dfrac{\partial L}{\partial i_{dref}} = 3 i_{dref} R_s + \lambda L_d \\[2mm] \dfrac{\partial L}{\partial i_{fref}} = 2 i_{fref} R_f + \lambda M_{sf} \\[2mm] \dfrac{\partial L}{\partial \lambda} = (L_d i_{dref} + M_{sf} i_{fref}) - \dfrac{\psi_{pm}(n_b - n_r)}{n_r} \end{cases} \tag{22}$$

In the formula, assuming that $\dfrac{\partial L}{\partial i_{dref}} = 0$, $\dfrac{\partial L}{\partial i_{fref}} = 0$, $\dfrac{\partial L}{\partial \lambda} = 0$, then the values of i_{dref} and i_{fref} are as following :

$$\begin{cases} i_{dref} = -\dfrac{L_d}{3R_s} \lambda \\[2mm] i_{fref} = -\dfrac{M_{sf}}{2R_f} \lambda \end{cases} \tag{23}$$

Where,

$$\lambda = \frac{6 R_s R_f \psi_{pm}(n_r - n_b)}{n_r (2 R_f L_d^2 + 3 R_s M_{sf}^2)} \tag{24}$$
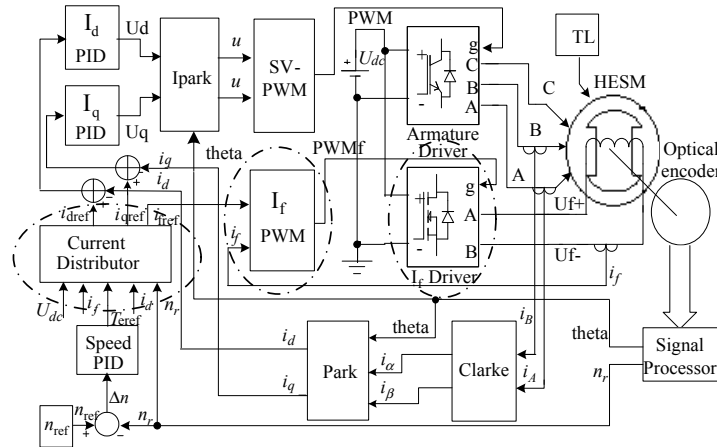
Fig. (2). The control system model of HESM.
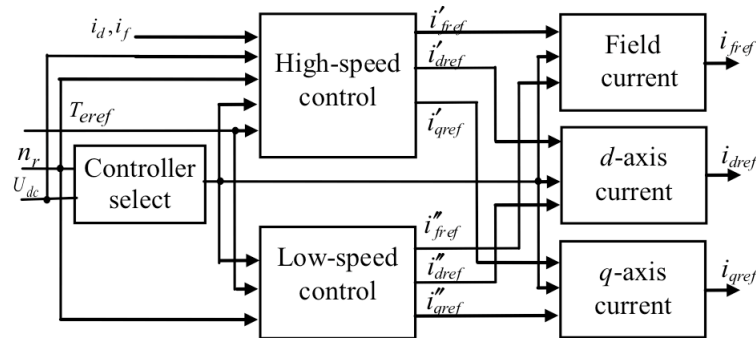
Fig. (3). Current allocation module.

In summary, two current allocation algorithms were used in the flux weakening control for the HESM.

Algorithm 1, adopted the flux-weakening control based on copper loss minimization algorithm, and the reference value for each current component are presented as follows.

$$
\begin{cases}
i_{\text{qref}} = k_i T_{\text{eref}} \\
i_{\text{dref}} = -\dfrac{L_d}{3R_s}\lambda \\
i_{\text{fref}} = -\dfrac{M_{sf}}{2R_f}\lambda
\end{cases}
\tag{25}
$$

Algorithm 2, used only the excitation current for flux weakening control, namely based on $i_{\text{dref}}=0$ vector control algorithm to adjust speed. From the equation (18) and (20), the current component reference values were obtained.

$$
\begin{cases}
i_{\text{qref}} = k_i T_{\text{eref}} \\
i_{\text{dref}} = 0 \\
i_{\text{fref}} = \dfrac{\psi_{pm}}{M_{sf}}\left(\dfrac{n_b}{n_r}-1\right)
\end{cases}
\tag{26}
$$

4. MODELING AND SIMULATION

In order to verify the effectiveness of flux weakening control method, simulation models of HESM were established by applied MATLAB/SIMULINK software, shown in Fig. (**2**). The main function modules include HESM, Clarke, Park, Ipark, Speed PID, Current Distributor, I_d PID, I_q PID, SVPWM, I_f PWM, Armature Driver, and I_f Driver module. Compared with the traditional PMSM vector control system, HESM control system adds 3 functional modules, I_f PWM, I_f Driver and Current Distributor. I_f PWM gives output control signal to the control I_f Driver which is a single-phase bridge inverter circuit. Current Distributor divides the entire operation region of HESM into a low speed zone and a high speed zone by using different partition control strategies. Its model is shown in Fig. (**3**). The control strategies of Current Distributor are used to coordinate allocation of the armature current and excitation current to realize reasonable distribution of the current reference values for the motor operations between two speed zones in enhanced or reduced flux state, to ensure stable, reliable, and efficient operational state of the motor.

According to the control system model shown in Fig. (**2**), the following simulation analysis was completed in detail. The simulation results of the three control methods were compared, which specifically included non-excitation current operation method, with only excitation current operation method and minimum copper loss method that used the d-

Table 1. Characteristic parameters of the prototype.

Parameters	Value	Parameters	Value
P_N (W)	700	U_{dc} (V)	300
n_N (rpm)	500	R_s (Ω)	2.7
T_N (Nm)	13	R_s (Ω)	33.0
I_N (A)	5	L_q(mH)	27
Ψ_{pm} (Wb)	0.243	M_{sf} (mH)	76
p	4	L_d (mH)	38
I_{fN} (A)	1.0	L_f (H)	0.57

Notes: I_{fN+} rated field enhancing excitation current; I_{fN-} rated field weakening excitation current.
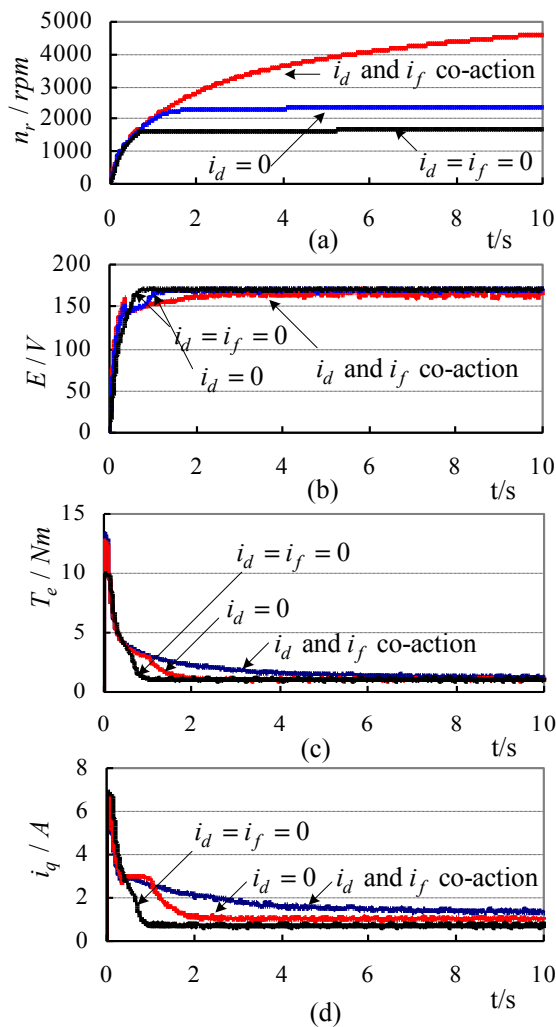
Fig. (4). Simulation waveforms of the HESM.

axis current and excitation current together for flux weakening operation. The simulation parameters of the HESM were set   according to the actual parameters of the prototype, shown in Table **1**.

Fig. (**4**) shows comparison of simulation waveform of HESM that used three kinds of control strategies: $i_{dref}=i_{fref}=0$, $i_{dref}=0$, and combined i_d and i_f for field weakening control to adjust speed. The HESM load was set to 1Nm, with the reference speed of 6000rpm.
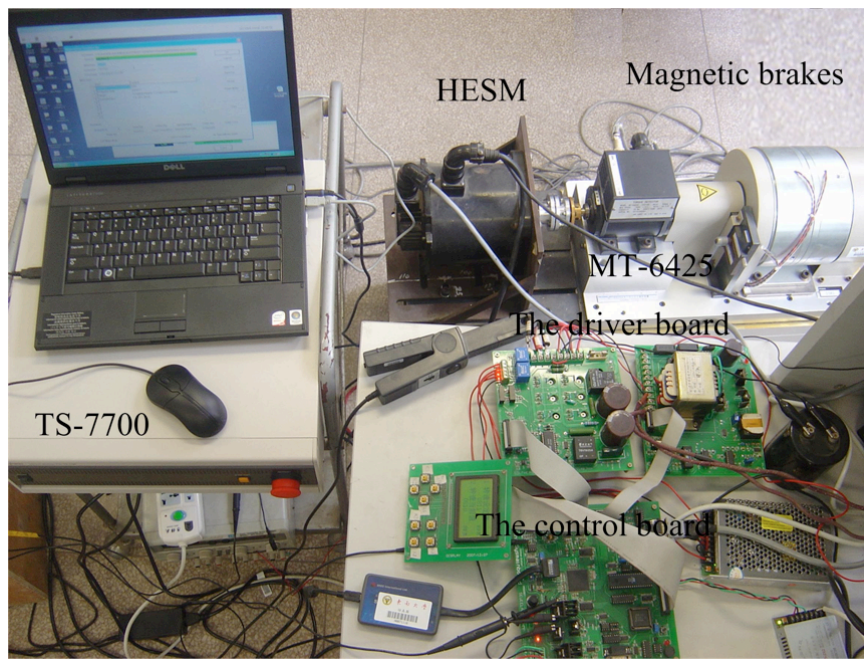
 Fig. (5). The experiment system of HESM.

Fig. (**4**) (a) shows the speed curve of HESM obtained by three different control methods. By adopting no excitation current control, the maximum speed observed was 1650rpm. i_f alone adjusted speed of flux weakening with the maximum speed of 2350rpm, and by combining i_d and i_f for flux weakening control, the maximum speed of HESM was observed to be more than 4600rpm.

Fig. (**4**) (b) shows the back EMF waveform of HESM under three different control methods. The back EMF with no field weakening current control reached fastest to the extreme, and flux weakening for adjusting speed and combined i_d and i_f increased the most slowly. Finally they became stable between 160V~170V.

Fig. (**4**) (c) shows   the i_q *vs* time curves obtained with three different control methods.

Fig. (**4**) (d) shows   the curve of the electromagnetic torque T_e changed with increase in the speed for three different control methods.

5. EXPERIMENTAL

According to the proposed control algorithms and the simulation results of HESM, the HESM controller based on TMS320F2812+AT89C55WD architecture was set up, and the corresponding motor drive experiment was carried out.

Fig. (**5**) shows the experimental picture of driving system for the HESM. Rated DC bus voltage for experimental prototype was 300V. The motor torque characteristics testing adopted TS-7700 Torque Station Pro with MT-6425 torque detectors. This set of equipment can be used to accurately measure the motor speed, torque, input and output power and efficiency *etc*. The prototype of HESM is an asymmetric interlaced construct, and an incremental optical

encoder disk, TAMAGAWA OIH48-2500, which is built in the motor. The architecture of control circuit board is based on TMS320F2812+ AT89C55WD. In addition, it includes two driving board of armature and excitation, and a control and display circuit board.

Fig. (**6**) shows the starting current waveforms of HESM with load 1Nm while the given speed was 2800rpm, greater than the flux weakening base speed (1270rpm) of the motor. In order to improve the starting torque of the motor, and for increased excitation winding inductance, a positively rated excitation current command was implemented to enhance the air-gap magnetic field before the armature current started at 0.5s. With the increase in the excitation current, motor speed decreased gradually. When the speed reached n_b, the rate of flux weakening control for adjusting speed increased, along with i_f and i_d which continually increased negatively with the rising speed .

Fig. (**7**) shows steady current waveforms in HESM weak magnetic operation. The given speed was 2800rpm, with the load torque of 1Nm and excitation current i_f of -0.8A, which basically remains   constant. Moreover, phase current was sine wave, amplitude was 4A, and the waveform was smooth with low harmonics.

Fig. (**8**) shows the curves of maximum output power in three different control strategies with changing speed. By adopting no field current mode ($i_d=i_f=0$), the speed was approximately up to 700~1300 r/min in the constant power region. In addition, only the excitation current i_f was used without d-axis current($i_d=0$) for regulating flux. The constant power region was extended to 450~1600 r/min while in the combined the d-axis current and the excitation current for regulating flux, the constant power region extended to 450~2000 r/min. However, when the speed exceeded to 2000
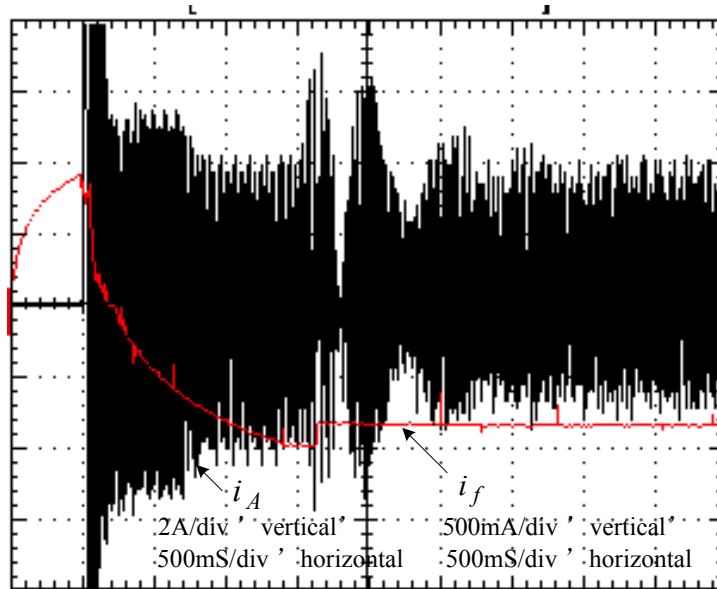
Fig. (6). Test waveforms of starting current.
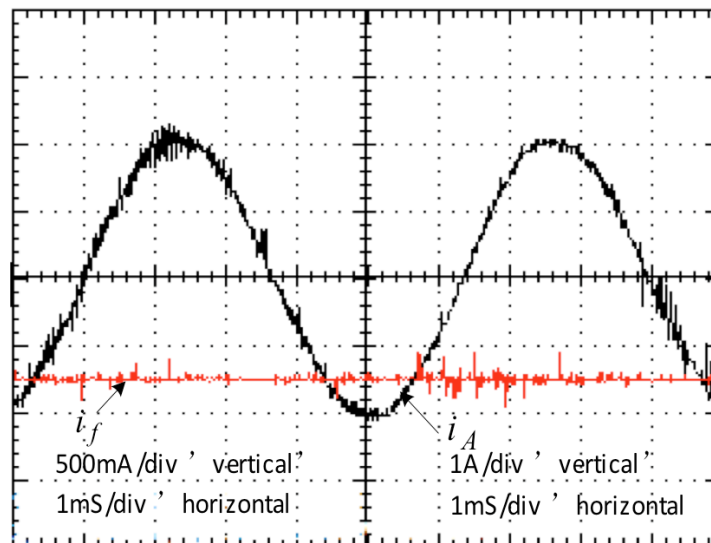
Fig. (7). Steady-state current waveforms in flux weakening operations.
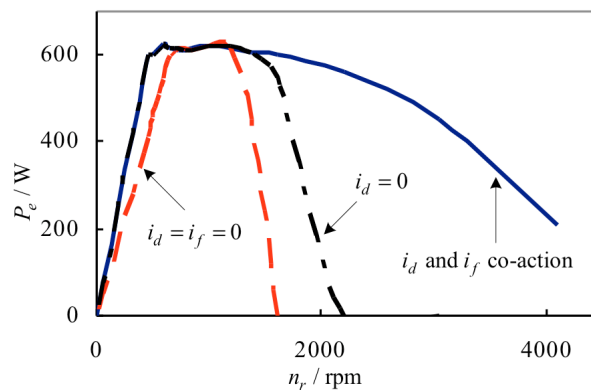
Fig. (8). Maximum output power at different speeds.

r/min, although the output power could not be kept constant, as it decreased slowly when the speed increased to 4000 r/min and the output power dropped to 200W. The experimental results show that applying the flux weakening control technology which combined i_d and i_f based on copper loss minimization control can effectively extend the speed range of HESM.

CONCLUSION

In this paper, according to the magnetic field adjusting property of HESM, based on the space voltage vector control, a new kind of two-speed-region control algorithm for HESM was presented. The proposed control method divided the whole speed range into two region. In the low speed region, the current control strategy was adopted with or without excitation current for adjusting speed according to the load torque while in the high speed region, the current control strategy with a combination strategy of holding q-axis components of Back-EMF unchanged and the copper loss minimization algorithm was adopted. Both simulation and experimental results were given to verify the validity of the proposed control strategy.

CONFLICT OF INTEREST

The authors confirm that this article content has no conflicts of interest.

ACKNOWLEDGEMENTS

REFERENCES

[1]   E. Spooner, S. W. Khatab, and N. G. Nicolaou, "Hybrid excitation of AC and DC machine", *Journal of University of Manchester Institute of Science and Technology*, vol. 3, pp. 48-52, 1989.

[2]   C. F. Yang, H. Y. Lin, J. Guo and Z. Q. Zhu, "Design and analysis of a novel hybrid excitation synchronous machine with asymmetrically stagger permanent magnet", *IEEE Transactions on Magnetics*, vol. 44, pp. 4353-4356, 2008.

[3]   C. C. Chan, K. T. Chau, and J. Z. Jiang, "Novel permanent magnet motor drives for electric vehicles," *IEEE Transactions on Industrial Electronics*, vol. 43, pp. 331-339, 1996.

[4]   J. J. Chen and K. P. Chin, "Minimum copper loss flux weakening control of surface mounted permanent magnet synchronous motors", *IEEE Transactions on Power Electronics*, vol. 18, no.4, pp. 929-936, 2003.

[5]   J. S. Lawler, J. Bailey, and J. McKeever, "Minimum current magnitude control of surface PM synchronous machines during constant power operation", *IEEE Power Electronics Letters*, vol. 3, no. 2, pp. 53-56, 2005.

[6]   E. F. Fuchs, and M. H. Myat, "Speed and torque range increases of electric drives through compensation of flux weakening", In: *International Symposium on Power Electronics, Electrical Drives, Automation and Motion*, Pisa, Italy, 2010, pp. 1569-1574.

[7]   J. J. Chen, and K. P. Chin, "Automatic flux-weakening control of permanent magnet synchronous motors using a reduced-order controller", *IEEE Transactions on Power Electronics*, vol. 15, no.5, pp. 881-890, 2000.

[8]   C. C. Chan, R. Zhang, and K. T. Chau, "Optimal efficiency control of PM hybrid motor drives for electrical vehicles", In: *28th Annual IEEE Power Electronics Specialists Conference*, pp. 363-368, 1997.

[9]   S. Shinnaka, "New dynamic mathematical model and new dynamic vector simulators of hybrid-field synchronous motors", *IEEE International Conference on Electric Machines and Drives*, pp. 882-889, 2005.

[10]   S. Shinnaka, "New optimal current control methods for energy-efficient and wide speed-range operation of hybrid-field synchronous motor", *IEEE Transactions on Industrial Electronics*, pp. 54, No. 5, pp. 2443-2450, 2007.

[11]   Q. F. Zhang, H. X. Wu, and S. K. Cheng, "Flux weakening control of axial and radial air-gap hybrid magnetic-circuit multi-coupling motor", *Journal of Harbin Institute of Technology*, vol. 38, no. 10, pp. 1654-1656, 2006 (in Chinese).

[12]   T. T. Zhu, Z. Q. Deng, and Y. Wang, "Research on hybrid-excited flux-switching machine and the current vector control strategy", In: *Proceedings of the CSEE*, vol. 32, no. 15, pp. 140-148, 2012. (in Chinese).

[13]   C. F. Yang, H. Y. Lin, and X. P. Liu, "Control strategy and simulation for hybrid excitation synchronous machine", *Electric Machines and Control*, vol. 12, no. 1, pp. 27-33, 2008. (in Chinese).